

Channel Propagation Characteristics for the Communications inside Tower Structure Buildings

Lugao Yin^{1, *}, Wenping Xie², Hao Huang¹, Xiaomin Chen², and Sheng Fang²

Abstract—Steel-tower structure buildings are different from traditional buildings and lack of effective channel models. A ray-based channel model suitable for severe multipath effects is proposed in this paper. The calculation method of channel parameters is introduced in detail, and the statistical characteristics at different frequencies are also analyzed based on the ray tracing (RT) method. We compare the RT-based channel data at 800 MHz, 2.4 GHz, 6 GHz, and 28 GHz with different positions of transceivers, and obtain the corresponding characteristics of channel parameters. According to the probability density distribution of each parameter, it is shown that the angle offset, delay, and power attenuation can be well fitted by Laplace distribution, Gaussian distribution, and exponential distribution, respectively. On this basis, the power delay profile at different positions is analyzed. These results can be used to optimize the deployment of sensor networks and evaluate the performance of communication systems inside the tower structure buildings.

1. INTRODUCTION

Nowadays, steel tower structures are applied in more and more buildings due to their good seismic, wind resistance ability, light weight, and strong toughness. Steel tower structures are used in many famous buildings, such as the Bird's Nest, National Centre for the Performing Arts of China, the Eiffel Tower, and Golden Gate Bridge. For the purpose of monitor or communication, we need to set up several sensors or network nodes inside the buildings. Since wireless channel plays an important role in data transmission and determines the communication quality significantly, it is important to study the channel model and characteristic inside the tower structure scenarios.

From the existing literatures, a lot of channel models have been studied in indoor or outdoor scenarios [1–7]. However, there are few studies for the inside of tower structures. Considering that tower structure is a special case of indoor scene, and some indoor channel models are worthy of references [8–12]. The channel model and channel characteristics were studied in metro train based on the ray tracing (RT) method at 26.5–40 GHz [9], and the validity of proposed model was verified by the measured data. In [10, 11], the channel in a cabin is studied. Besides, the authors in [10] also proposed a path loss prediction scheme combining empirical model and machine learning based on the measured data of 2.4 GHz, 3.52 GHz, and 5.8 GHz. Some scholars studied the channels inside the ships [12]. Similar to tower structures, bulk carrier vessel has a high metal content, so the influence of metal environments on the path loss was studied in the literature [12].

However, tower structure has some unique features, such as massive reflective surfaces and serious multipath effect. Moreover, tower structure is not a fully enclosed structure, and some reflected signals are lost. In this paper, a ray-based channel model is proposed. Based on RT method, the propagation

Received 26 March 2021, Accepted 7 June 2021, Scheduled 2 July 2021

* Corresponding author: Lugao Yin (yinlugao32@163.com).

¹ Beijing Institute of Astronautical Systems Engineering, Beijing 100076, China. ² The Key Laboratory of Dynamic Cognitive System of Electromagnetic Spectrum Space, Ministry of Industry and Information Technology, Nanjing University of Aeronautics and Astronautics, Nanjing, Jiangsu 211100, China.

path of each ray can be tracked. By calculating the geometric parameters and model parameters of each ray, statistical parameters such as angle offset, delay, and power attenuation can be obtained. In addition, in order to reduce the computational complexity under the premise of ensuring accuracy, the rays with less power are ignored. On this basis, the characteristics of channel parameters are analyzed. The distribution of each model parameters is counted, and the distribution is fitted with appropriate functions.

The remainder of the paper is organized as follows. Section 2 gives a general ray-based channel model for the tower structure buildings. In Section 3, channel parameters such as angle, delay, and power are given. The simulation results and analysis are shown in Section 4. Finally, conclusions are given in Section 5.

2. CHANNEL MODEL FOR TOWER STRUCTURE SCENES

The communication channel inside steel structure buildings is complex. The received signal is composed of multipath components, which are represented by angle, time delay, and power gain. The channel impulse response (CIR) can be modeled as the sum of many rays as

$$h(t, \tau, \alpha, \beta) = \sum_{l=0}^L A_l e^{j\psi_l} \delta(t - \tau_l) \delta(\alpha^{\text{TX}} - \alpha_l^{\text{TX}}) \delta(\beta^{\text{TX}} - \beta_l^{\text{TX}}) \delta(\alpha^{\text{RX}} - \alpha_l^{\text{RX}}) \delta(\beta^{\text{RX}} - \beta_l^{\text{RX}}) \quad (1)$$

where L is the number of rays; A_l , ψ_l , and τ_l denote the power gain, random initial phase, and delay of the l th ray, respectively; and α_l^{TX} , β_l^{TX} , α_l^{RX} , and β_l^{RX} denote the azimuth angle of departure (AAoD), elevation angle of departure (EAoD), azimuth angle of arrival (AAoA), and elevation angle of arrival (EAoA), respectively. In addition, δ function represents the unit impulse response. Therefore, the normalized direction vector of the transmitting/receiving signal of l th ray can be represented as

$$\mathbf{r}_l^{\text{TX/RX}} = \left[\cos \beta_l^{\text{TX/RX}} \cos \alpha_l^{\text{TX/RX}}, \cos \beta_l^{\text{TX/RX}} \sin \alpha_l^{\text{TX/RX}}, \sin \beta_l^{\text{TX/RX}} \right] \quad (2)$$

Note that $l = 0$ denotes the light-of-sight (LoS) ray, otherwise, non-light-of-sight (NLoS) rays.

There are many methods for calculating channel parameters theoretically based on the electromagnetic theory. For example, by transforming the curl equation of Maxwell's equations in time domain into a finite difference time domain (FDTD) equation on a discrete grid node, the propagation process in the desired region can be intuitively simulated by iteration in time domain. This model is called FDTD [13]. This method has high accuracy as well as complexity. Since the analysis of tower structure channel characteristics does not need extremely accurate solution, the geometric optics theory combined with the electromagnetic propagation theory is applied in this paper.

3. MODEL PARAMETER COMPUTATION AND ANALYZE

The ray tracing method based on Geometric Optics (GO) theory and Geometric Theory of Diffraction (GTD) is a deterministic parameter estimation method, which has been widely used in recent years [14]. The RT method can calculate every reflection, scattering, and diffraction of the ray, calculate whether there is an intersection point on the surface of the scatterer, and finally carry out vector superposition on all the ray signals at the receiver. Considering the complex internal structure of the tower, there are not only direct rays, but also a lot of reflected and diffracted rays, and the positions of the transmitter and receiver remain unchanged. RT method is more suitable to analyze. We divide all parameters into geometric parameters and model parameters. The calculation details of each parameter are as follows.

3.1. Geometric Parameters

We set the coordinates of the transmitter and receiver, project the ray from the transmitter to the triangle facet, and judge whether there is an intersection point between the ray and the triangle facet. Then the coordinates of the intersection point and the total distance of the ray can be obtained [15]. Firstly, we assume that the coordinate of TX antenna is $\text{TX} = (\text{TX}_x, \text{TX}_y, \text{TX}_z)$, and the coordinate

of RX antenna is $RX = (RX_x, RX_y, RX_z)$. According to geometric theory, the transmission distance of LoS ray can be calculated as

$$D_0^{TX,RX} = \sqrt{(TX_x - RX_x)^2 + (TX_y - RX_y)^2 + (TX_z - RX_z)^2} \quad (3)$$

For the case of NLoS rays, the coordinate $Q_l = (Q_{l,x}, Q_{l,y}, Q_{l,z})$ of the intersection point of l th ray and the scatterer can be obtained by the algorithm of trigonometry, and then the distance between TX antenna and scatterer $D_l^{TX,S}$ and the distance between scatterer and Rx $D_l^{S,RX}$ can be respectively expressed as

$$D_l^{S,RX} = \sqrt{(RX_x - Q_{l,x})^2 + (RX_y - Q_{l,y})^2 + (RX_z - Q_{l,z})^2} \quad (4)$$

$$D_l^{TX,S} = \sqrt{(TX_x - Q_{l,x})^2 + (TX_y - Q_{l,y})^2 + (TX_z - Q_{l,z})^2} \quad (5)$$

3.2. Channel Parameters

Based on the geometric parameters, the coordinates of the transmitter, receiver, and the intersection point of the ray and triangular facet are obtained. We can calculate the channel parameters according to the definitions in [2].

The angle parameter of the channel is related to the position vector of the TX antenna, RX antenna, and scatterers. For all valid rays received by the RX, AAoD α_l^{TX} and EAoD β_l^{TX} can be expressed as

$$\alpha_l^{TX} = \arctan\left(\frac{Q_y - TX_y}{Q_x - TX_x}\right) \quad (6)$$

and

$$\beta_l^{TX} = \frac{\pi}{2} - \arccos\left(\frac{Q_z - TX_z}{\sqrt{(TX_x - Q_{l,x})^2 + (TX_y - Q_{l,y})^2 + (TX_z - Q_{l,z})^2}}\right) \quad (7)$$

Similarly, AAoA α_l^{RX} and EAoA β_l^{RX} can be expressed as

$$\alpha_l^{RX} = \arctan\left(\frac{RX_y - Q_y}{RX_x - Q_x}\right) \quad (8)$$

and

$$\beta_l^{RX} = \frac{\pi}{2} - \arccos\left(\frac{RX_z - Q_z}{\sqrt{(RX_x - Q_{l,x})^2 + (RX_y - Q_{l,y})^2 + (RX_z - Q_{l,z})^2}}\right) \quad (9)$$

In particular, when there is a LoS ray between the TX antenna and RX antenna, the formula for α_l^{TX} and β_l^{TX} can be obtained by replacing the coordinate of Q_l in Equations (6) and (7) with the coordinate of RX. Similarly, the formula for α_l^{RX} and β_l^{RX} can be obtained by replacing the coordinate of Q_l in Equations (8) and (9) with the coordinate of TX antenna.

Since the total transmission distance of each effective ray is different, the corresponding time delay of the ray can be calculated by calculating the total distance of each ray. Assume that c is the propagation velocity of electromagnetic wave in free space, then the delay of rays can be calculated as

$$\tau_l = \frac{D_l^{TX,S} + D_l^{S,RX}}{c} \quad (10)$$

In particular, when there is a LoS ray between the TX antenna and RX antenna, the delay of LoS ray can be calculated as

$$\tau_0 = \frac{D_0^{TX,RX}}{c} \quad (11)$$

The total field intensity of the receiving point is the vector superposition of the field intensity of the direct, reflected, and diffracted rays arriving at the receiving point. Assuming that the transmitting

antenna gain and receiving antenna gain are G^{TX} and G^{RX} , respectively, the power gain of the receiving point can be expressed as

$$A_l = 20 \lg \left(G^{\text{TX}} G^{\text{RX}} \left(\frac{\lambda}{4\pi} \right)^2 \left| \frac{\mathbf{E}_l}{\mathbf{E}^{1m}} \right| \right) \quad (12)$$

where λ is the wavelength, \mathbf{E}^{1m} the electric field intensity of 1 m from the transmitter, and \mathbf{E}_l the receiving field strength of l th ray.

For the LoS case, the calculation formula of electric field intensity can be described as

$$\mathbf{E}_l = \mathbf{E}^{1m} \frac{e^{-j \frac{D_0^{\text{TX,RX}}}{\lambda}}}{D_0^{\text{TX,RX}}} \quad (13)$$

For the reflection ray, assuming that reflection coefficient is R , the calculation formula of electric field intensity can be described as

$$\mathbf{E}_l = \mathbf{E}^{1m} R \frac{e^{-j \frac{D_l^{\text{TX,S}} + D_l^{\text{S,RX}}}{\lambda}}}{D_l^{\text{TX,S}} + D_l^{\text{S,RX}}} \quad (14)$$

Similarly, when there are diffraction rays, according to the UTD theory, assuming that diffraction coefficient is D , the electric field intensity can be calculated as

$$\mathbf{E}_l = \mathbf{E}^{1m} D \sqrt{\frac{D_l^{\text{TX,S}}}{D_l^{\text{S,RX}} (D_l^{\text{TX,S}} + D_l^{\text{S,RX}})}} e^{-j \frac{D_l^{\text{TX,S}} + D_l^{\text{S,RX}}}{\lambda}} \quad (15)$$

4. SIMULATION RESULTS AND STATISTICAL CHARACTERISTIC

We conducted simulation inside the tower structure scenario based on the RT method. As shown in Fig. 1, the TX antenna is placed on the edge of the tower structure at the height of 53 m, and the

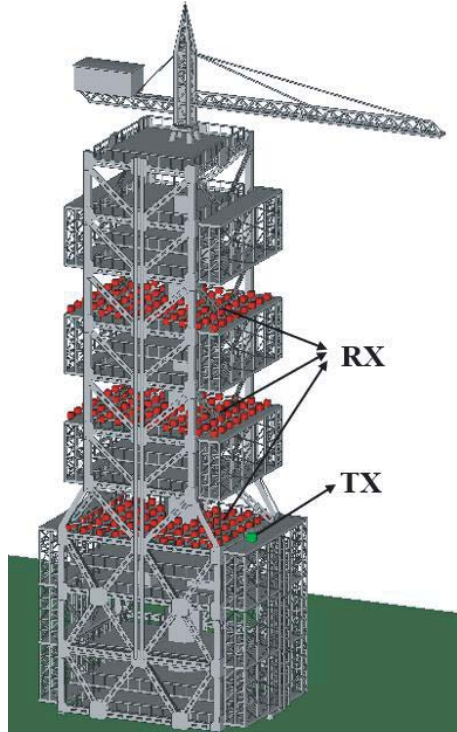


Figure 1. Communication in tower structure scenario.

RX antenna is placed on three floors with heights of 52 m, 84 m, and 114 m, respectively. There are 80 receiving nodes on each floor, and the distance between each two adjacent receiving nodes is 5 meters. In addition, in order to illustrate the effect of communication frequency on the channel parameters and statistical properties, we set four different frequencies as 800 MHz, 2.4 GHz, 6 GHz, and 28 GHz. The rest simulation parameters are described in Table 1. Finally, we obtain up to 960 channel data from different channels at different locations and frequencies, including angle, delay, and power. Based on these data, the statistical characteristics are analyzed as follows.

Table 1. Simulation parameters.

Parameter	Value
Frequency	800 MHz, 2.4 GHz, 6 GHz, 28 GHz
Bandwidth	500 MHz
Transmitting power	20 dBm
Antenna type	Isotropic antenna
TX antenna location	53 m
RX antenna location	52, 84, 114 m

In order to investigate the distribution characteristics of angle parameters, the angle values of all rays from different positions are subtracted from their mean values. Taking AAoD as an example, the statistical results of azimuth angle offset at different operating frequencies and different heights are shown in Fig. 2. The azimuth angle offset is defined as the azimuth of each ray minus the average of the azimuth angles of all rays. It can be observed that when the transmitter and receiver are at the same altitude, the variance of the azimuth angle offset decreases from 0.88 to 0.68 as the frequency increases. However, when the receiver height is 114 m, the variance of the azimuth angle offset increases from 0.86 to 1.28 with the increase of frequency. This indicates that with the increase of frequency, the influence of multipath effect on signal propagation becomes more and more serious. Moreover, it can be seen that the azimuth offset distribution can be fitted well with the Laplace function [16], and the mean μ_a and standard deviation σ_a of the fitted curves are shown in Table 2.

Since the delay has a great influence on the communication quality, we count the delay of each effective received ray, and the distribution is shown in Fig. 3. With the increase of the height, the number of reflections for the rays to reach the RX increases. It is found that the delay distribution can be fitted by Gaussian distribution. The mean μ_τ and standard deviation σ_τ of fitting curve at different heights and frequencies are shown in Table 2. When the receiver height is 52 m, the mean of the delay distribution changes greatly with the increase of frequency, from 174.9 ns to 208.6 ns, and the variance decreases from 89.32 to 85.36. When the height of the receiver is 84 m and 114 m, the mean and variance of the delay distribution basically remain unchanged with the increase of frequency. Note that there are a lot of reflected and scattered rays inside the tower structure building due to the rich scattering, and the parameter characteristics are different from other scenes.

The attenuation of received power is also important for assessing the quality of communication channel. In order to eliminate the influence of received power of the LoS ray, we evaluate the value of power attenuation instead of the absolute received power. The distribution of power attenuation is shown in Fig. 4. We find that the power attenuation of most rays is concentrated in the range of 0 ~ 5 dBm, and only a few rays have power attenuation over 20 dBm. Therefore, in the analysis and calculation, in order to reduce the computational complexity, the ray with less power can be ignored. Furthermore, the PDFs of power attenuation can be fitted well by the exponential distribution, and the attenuation coefficients λ_P and standard deviation σ_P of each frequency at each height are shown in Table 2.

In order to observe the received signal power and delay of individual typical positions, we select a position for each floor, which is denoted as Rx1, Rx2, and Rx3, respectively. Fig. 5 shows the power delay profile at the above three receiving terminals at 800 MHz with the same TX. It can be seen that

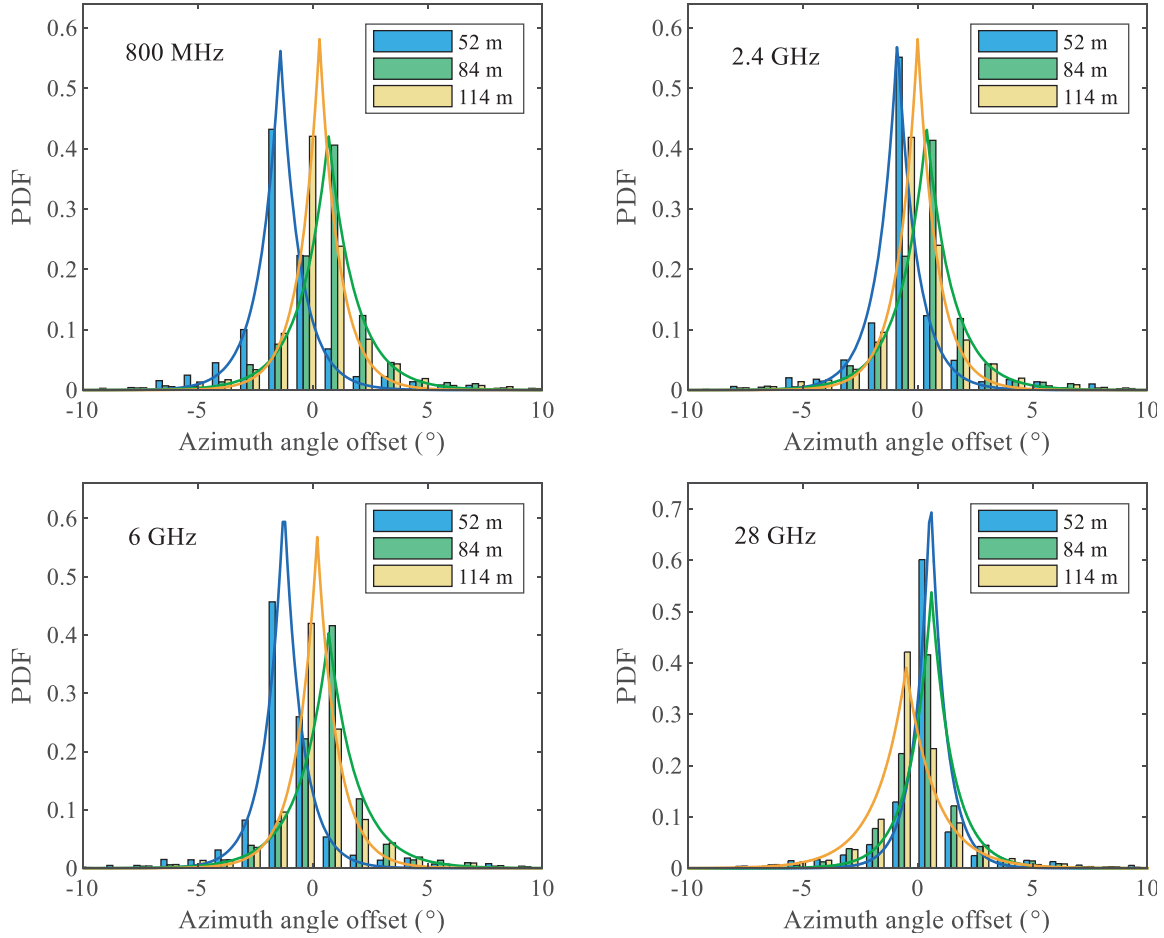
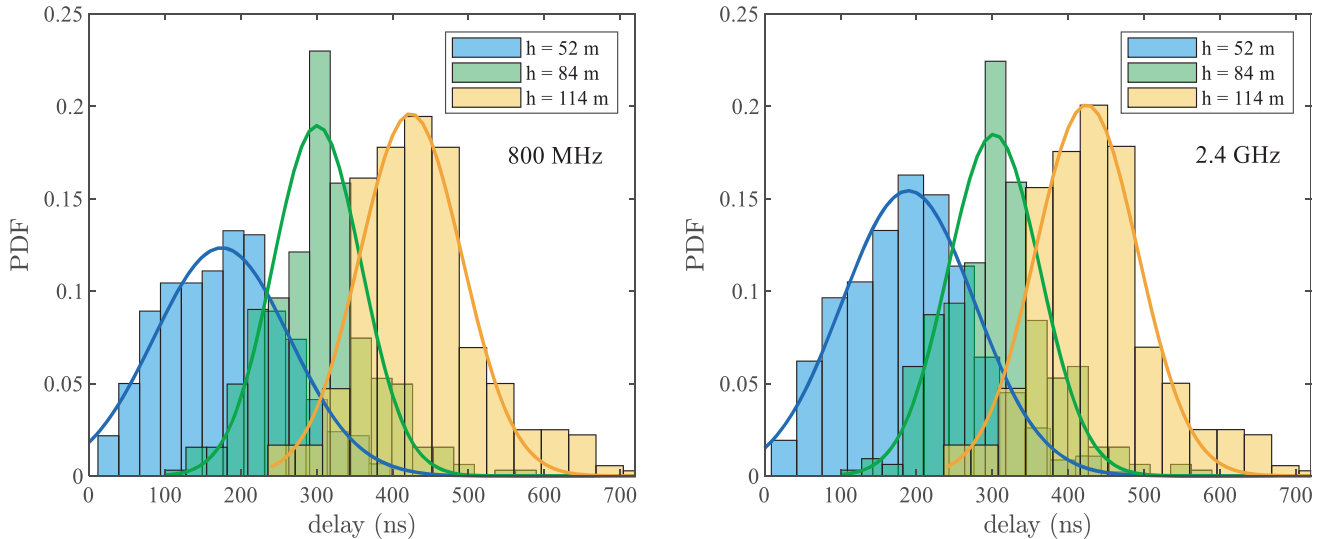


Figure 2. Statistical distributions of azimuth angle offset.

the signal propagation is greatly affected by the distance and position. Due to the existence of LoS ray between Rx1 and TX, the signal received by Rx1 has a smaller delay and a higher power than the one received by Rx2 and Rx3. In addition, due to the particularity of tower structure, there are a large number of reflected and scattered rays at the receiver.



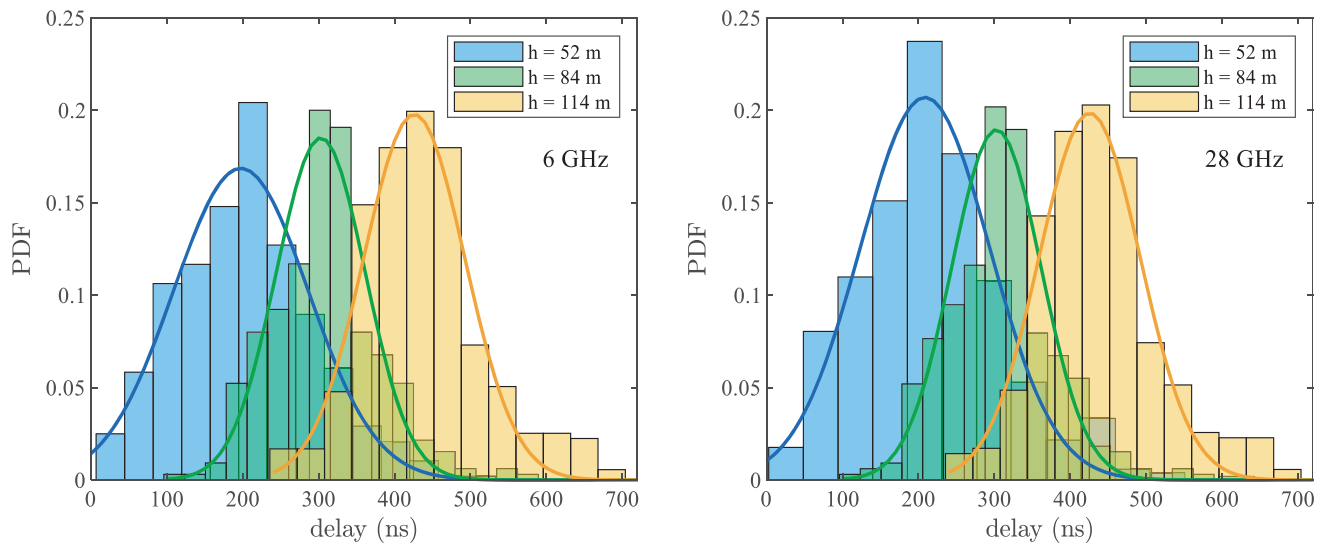


Figure 3. Statistical distributions of ray delay.

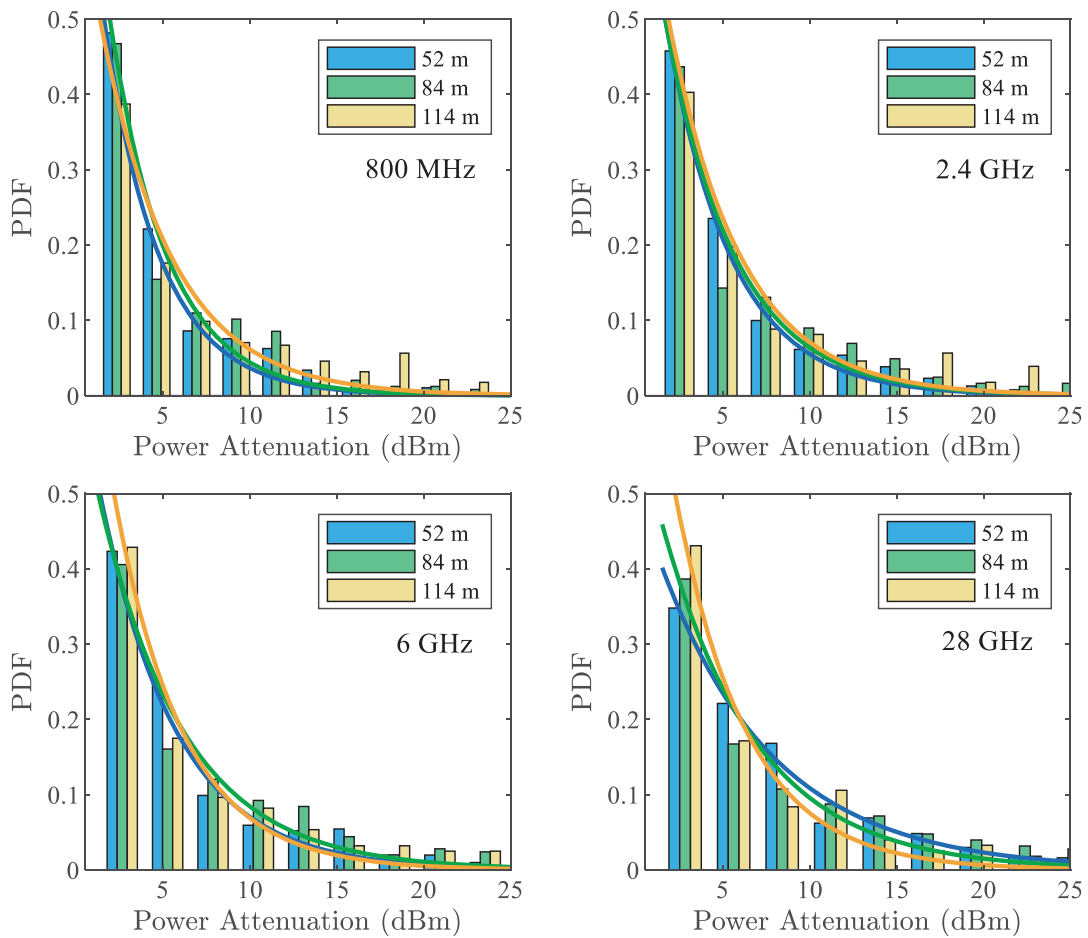
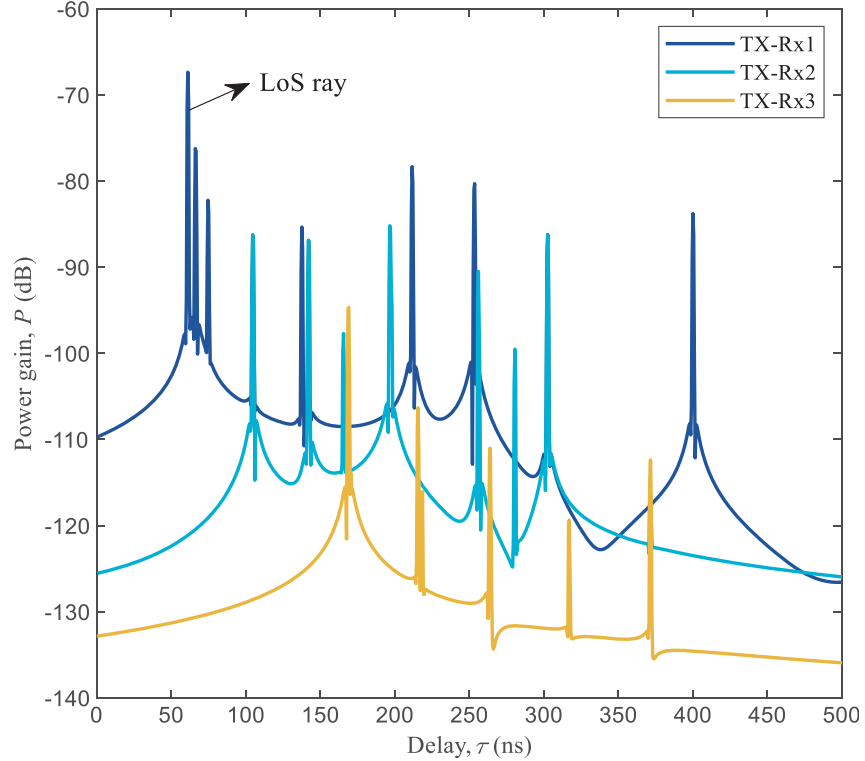


Figure 4. Statistical distributions of power attenuation.

Table 2. Fitting parameters of angle, delay and power.

Channel parameters	Height	Curve parameters	Frequencies			
			800 MHz	2.4 GHz	6 GHz	28 GHz
Azimuth angle offset	52 m	μ_a	-1.41	-0.88	-1.25	0.56
		σ_a	0.88	0.86	0.79	0.68
	84 m	μ_a	0.69	0.39	0.7	0.6
		σ_a	1.18	1.15	1.24	0.93
	114 m	μ_a	0.3	0	0.2	-0.5
		σ_a	0.86	0.86	0.88	1.28
Delay	52 m	μ_τ	174.9	189.3	197.5	208.6
		σ_τ	89.32	87.69	88.89	85.36
	84 m	μ_τ	300.6	302.2	302.8	302.7
		σ_τ	58.01	60.49	58.64	58.98
	114 m	μ_τ	423.9	424.2	425.9	425.5
		σ_τ	67.60	67.47	66.74	66.72
Power attenuation	52 m	λ_P	0.82	0.78	0.68	0.51
		σ_P	1.49	1.64	2.16	3.84
	84 m	λ_P	0.89	0.75	0.65	0.61
		σ_P	1.26	1.78	2.37	2.69
	114 m	λ_P	0.69	0.78	0.86	0.86
		σ_P	2.10	1.64	1.35	1.35

**Figure 5.** Power delay profile of different Rx positions.

5. CONCLUSIONS

In this paper, we have developed a ray-based channel model suitable for severe multipath effects and analyzed channel characteristics. Based on a large amount of RT-based channel data, we have obtained the distributions of azimuth angle offset, delay, and power attenuation at three heights and four carrier frequencies. The simulation results show that as the height changes, the frequency will have different effects on different parameters of the channel. However, the statistical characteristics of the channel parameters remain unchanged. The angle offset, delay, and power can be well fitted with Laplace function, Gaussian distribution, and exponential distribution, respectively. This is of great significance for us to establish channel models and evaluate the performance of communication systems. The model and parameter calculation method established in this paper can be used in tower structure buildings or other scenes with many metal scatterers.

REFERENCES

1. Ko, J., Y. Cho, S. Hur, T. Kim, J. Park, et al., "Millimeter-wave channel measurements and analysis for statistical spatial channel model in in-building and urban environments at 28 GHz," *IEEE Transactions on Wireless Communications*, Vol. 16, No. 9, 5853–5868, Sept. 2017.
2. Jiang, S., Q. Zhu, C. Wang, K. Mao, W. Xie, et al., "Map-based UAV mmWave channel model and characteristics analysis," *2020 IEEE/CIC International Conference on Communications in China (ICCC Workshops)*, 23–28, Chongqing, China, 2020.
3. Zhu, Q., S. Jiang, C. Wang, B. Hua, K. Mao, et al., "Effects of digital map on the RT-based channel model for UAV mmWave communications," *2020 International Wireless Communications and Mobile Computing (IWCMC)*, 1648–1653, Limassol, Cyprus, 2020.
4. Cheng, L., Q. Zhu, C. Wang, W. Zhong, B. Hua, et al., "Modeling and simulation for UAV air-to-ground mmWave channels," *2020 14th European Conference on Antennas and Propagation (EuCAP)*, 1–5, Copenhagen, Denmark, 2020.
5. Khawaja, W., O. Ozdemir, F. Erden, I. Guvenc, and D. W. Matolak, "Ultra-wideband air-to-ground propagation channel characterization in an open area," *IEEE Transactions on Aerospace and Electronic Systems*, Vol. 56, No. 6, 4533–4555, Dec. 2020.
6. Perez, A., A. Fouda, and A. S. Ibrahim, "Ray tracing analysis for UAV-assisted integrated access and backhaul millimeter wave networks," *2019 IEEE 20th International Symposium on "A World of Wireless, Mobile and Multimedia Networks" (WoWMoM)*, 1–5, Washington, DC, USA, 2019.
7. Zhou, A., J. Huang, J. Sun, Q. Zhu, C. Wang, et al., "60 GHz channel measurements and ray tracing modeling in an indoor environment," *2017 9th International Conference on Wireless Communications and Signal Processing (WCSP)*, 1–6, Nanjing, China, 2017.
8. Chandra, A., A. Rahman, U. Ghosh, J. García-Naya, A. Prokeš, et al., "60-GHz millimeter-wave propagation inside bus: Measurement, modeling, simulation, and performance analysis," *IEEE Access*, Vol. 7, 97815–97826, 2019.
9. He, D., K. Guan, J. G. Loygorri, B. Ai, X. Wang, et al., "Channel characterization and hybrid modeling for millimeter-wave communications in metro train," *IEEE Transactions on Vehicular Technology*, Vol. 69, No. 11, 12408–12417, Nov. 2020.
10. Wen, J., Y. Zhang, G. Yang, Z. He, W. Zhang, "Path loss prediction based on machine learning methods for aircraft cabin environments," *IEEE Access*, Vol. 7, 159251–159261, 2019.
11. Cogalan, T., S. Videv, and H. Haas, "Aircraft in-cabin radio channel characterization: From measurement to model," *GLOBECOM 2017 — 2017 IEEE Global Communications Conference*, 1–6, Singapore, 2017.
12. De Beelde, B., E. Tanghe, M. Yusuf, D. Plets, E. De Poorter, et al., "60 GHz path loss modelling inside ships," *2020 14th European Conference on Antennas and Propagation (EuCAP)*, 1–5, Copenhagen, Denmark, 2020.

13. Shi, Z., P. Xia, Z. Gao, L. Huang, and C. Chen, "Modeling of wireless channel between UAV and vessel using the FDTD method," *10th International Conference on Wireless Communications, Networking and Mobile Computing (WiCOM 2014)*, 100–104, Beijing, 2014.
14. Lee, J., J. Choi, and S. Kim, "Cell coverage analysis of 28 GHz millimeter wave in urban microcell environment using 3-D ray tracing," *IEEE Transactions on Antennas and Propagation*, Vol. 66, No. 3, 1479–1487, Mar. 2018.
15. Liu, Z., D. Shi, Y. Gao, C. Yuan, J. Bi and Z. Tan, "A New Ray Tracing Acceleration Technique in the Simulation System of Electromagnetic Situation," 2015 7th Asia-Pacific Conference on Environmental Electromagnetics (CEEM), 2015, 329-333, doi: 10.1109/CEEM.2015.7368698.
16. Q. Zhu, C. Wang, B. Hua, K. Mao, S. Jiang, et al., *3GPP TR 38.901 Channel Model, The Wiley 5G Ref: The Essential 5G Reference Online*, Wiley Press, Jan. 26, 2021, ISBN: 9781119471509.